polymer papers

Vibrations of crystallographic defects associated with a single chain in polyethylene

D. H. Reneker and J. Mazur
Center for Materials Science, National Bureau of Standards, Washington, DC 20234, USA
(Received 25 January 1984)

The vibrational behaviour of crystallographic defects associated with a single chain were investigated for a dispiration, disclination, and dislocation in polyethylene. An approximate longitudinal modulus for the defects was determined by using conformational calculations to estimate the energy changes associated with changes in the length of a defect. This modulus, combined with the mass per unit length of the defect, was used to estimate the lowest longitudinal frequency of the defect, which was found to be around 100 cm^{-1} for all the defects considered. Normal mode vibrational calculations for oligomers containing defects showed that the predicted lowest longitudinal modes could be identified by examination of the displacements associated with modes occurring in the estimated frequency range. It was shown that the defects could be considered as localized oscillators embedded in the crystal and coupled to the vibrational modes of the crystal. The presence of defects provides special mechanisms for coupling light waves and lattice vibrations in the crystal which may affect the Raman spectrum.

(Keywords: crystal vibrations; defect vibrations; disclination; dislocation; dispersion relations; dispiration; longitudinal mode; polyethylene crystals)

INTRODUCTION

Some of the effects of a particular crystallographic defect associated with a single chain and called a dispiration[1] on the longitudinal acoustic mode or LAM of crystalline polyethylene were described by Reneker and Fanconi[2]. The impetus for that work was to provide an explanation for the decrease in the integrated Raman intensity of the longitudinal acoustic mode with increasing temperature that was first observed by Koenig and Tabb[3] and later by Snyder *et al.*[4]. Reneker and Fanconi[2] suggested that the decrease in Raman intensity resulted from the fact that the effective modulus associated with displacements along the chain axis is much lower for a defect than is the case for a planar zigzag chain conformation. In a defect, displacements occur which lead to the deformation of torsional coordinates and to changes in the intermolecular distances. The change in the potential energy which accompanies the changes in these coordinates is smaller than for longitudinal extension or compression of a zigzag chain. It was found in the present work that the changes in the interatomic distances between the defect and the surrounding chains in the deformed lattice provide the largest contribution to the value of the effective longitudinal modulus. Generally higher moduli were calculated by McCullough *et al.*[5] for short non-planar zigzag sequences with intermolecular interactions neglected.

The effect of the lower modulus associated with the defects is more pronounced in the low frequency vibrations since they involve primarily skeletal deformations. In this paper the low frequency vibrations of crystallographic defects associated with single chains are investigated. Since the ends of the defect are attached to planar zigzag segments, it is necessary to consider the coupling of defect vibrations to vibrations of the planar zigzag segments. This is done with the aid of the frequency–dispersion curves for the polyethylene lattice.

Frequency–dispersion curves based on the crystal model are used to calculate minimum energy conformations of defects and other lattice models. For the phonons which propagate in the chain direction, dispersion curves for orthorhombic and triclinic lattices are from the review paper by Barnes and Fanconi[6]. Dispersion curves for phonons which propagate in directions other than the chain direction are from the review paper by Kitagawa and Miyazawa[7]. Analysis of the dispersion curves shows the possibility of defect vibrations coupling to lattice modes propagating not only along the chain stem axis, but also in other directions.

In the first part of the paper a 'static' modulus is calculated for the defect region by observing the change in the defect energy as the defect is shortened or lengthened in small increments. The defect itself is then considered as an elastic rod with the calculated modulus and a density near that of polyethylene. This leads to an estimate of the lowest longitudinal frequency of an isolated defect. The next section deals with the detailed vibrational normal mode calculations of defect containing oligomers either 10, 15 or 21 carbon atoms long.

A defect, (either a dispiration or a disclination), was placed at various positions along the chain. Dislocations were numerically unstable in the modulus calculations with the short oligomers used, but would clearly behave in a similar manner. Analysis of the atomic displacements for the modes in the low frequency range showed that the displacements in the defect region were encompassed in a

0032-3861/84/111549-13$03.00

general way by simple theoretical arguments and predictions. The defects tend to vibrate at their own natural frequencies and to couple to normal modes of the polyethylene crystal that have the same frequency. The last section of the paper deals with the calculated Raman intensities of the defect vibrations. The calculations, based on the bond polarizability method, show that the Raman intensity associated with the lowest longitudinal frequency of the defect might contribute to the observed[8] intense irregular background in the Raman spectrum in the frequency region of 85 cm^{-1} to 105 cm^{-1}.

I. ELASTIC DEFORMATION OF DEFECTS, VIA STATIC CALCULATIONS

(a) *Description of calculations*

The static calculations of the modulus were performed by moving the two terminal atoms of a defect toward each other along the chain axis by small increments and calculating the defect energy after each increment. The terminal atoms are identified as those encompassing virtually the entire defect. In the dispiration and dislocation the two forced atoms enclose a 7-bond segment and in the disclination, a 6-bond segment. The only constrained coordinates are the longitudinal positions of the terminal atoms. All others are free to move in any direction. The two perpendicular directions of the forced atoms are also free to adjust themselves. At each step, the entire system consisting of a central, defect-containing chain plus the six chains of the inner shell, was energy-minimized. The packing energy program employed in the current calculations was described in detail in ref. 9.

For the dispiration, the same calculation was repeated for tensile forces, that is, the terminal atoms were displaced away from each other. All calculations were performed on 21 carbon atom oligomers. For the dispiration, the calculations were repeated on shorter, 15 carbon atom oligomers in order to evaluate contributions to the static modulus associated with parts of the chain outside the defect. Such contributions were small.

A few comments should be made about the starting defect conformations employed in conjunction with present calculations, both static and dynamic. The defect conformations reported previously[1] were artificially constrained at the ends of the defect-bearing 21 carbon atom oligomers, so that they fit into the lattice and there was no mismatch as the chain continued into the crystal. These constraints were removed to minimize the energy changes outside the defect when the defect is statically deformed and to perform simultaneous calculations of the normal mode vibrations.

The conformation of the dispiration changed only slightly upon the removal of the constraints at the chain ends. However, the disclination changed considerably. It assumed a more compact arrangement (see *Figure 1*). The entire 360° of twist was confined within a short segment. This indicates that the forces that were previously applied to the ends of the model chain, to insure that parts of the chain outside the defect fit into the lattice were in a direction that tended to extend the disclination. The compact form of the disclination is more stable in a short alkane crystal, while in a longer molecule the more extended gentle twist of 180° combined with a compact 180° twist is more stable[1]. This suggests the possibility that in a crystal with very long stems a disclination might have 360° of gentle twist with no dihedral angles near the *gauche* conformation. The modulus of the gentle twist would approach the higher value associated with the zigzag conformation, with little effect on the longitudinal acoustic mode intensity as reported in ref. 2.

For the dislocation, removal of constraints causes the defect to transform into a partial dislocation (with only one extra CH_2 group). A different procedure was necessary in this case. Starting with the oligomer initially constrained at each ends, these constraints were removed from the chain-terminal atoms at the same time as the displacements were applied to the defect. For the dislocation the calculated energy change *versus* squared strain for both extension and compression fell on the same line since the minimum energy conformation could not be

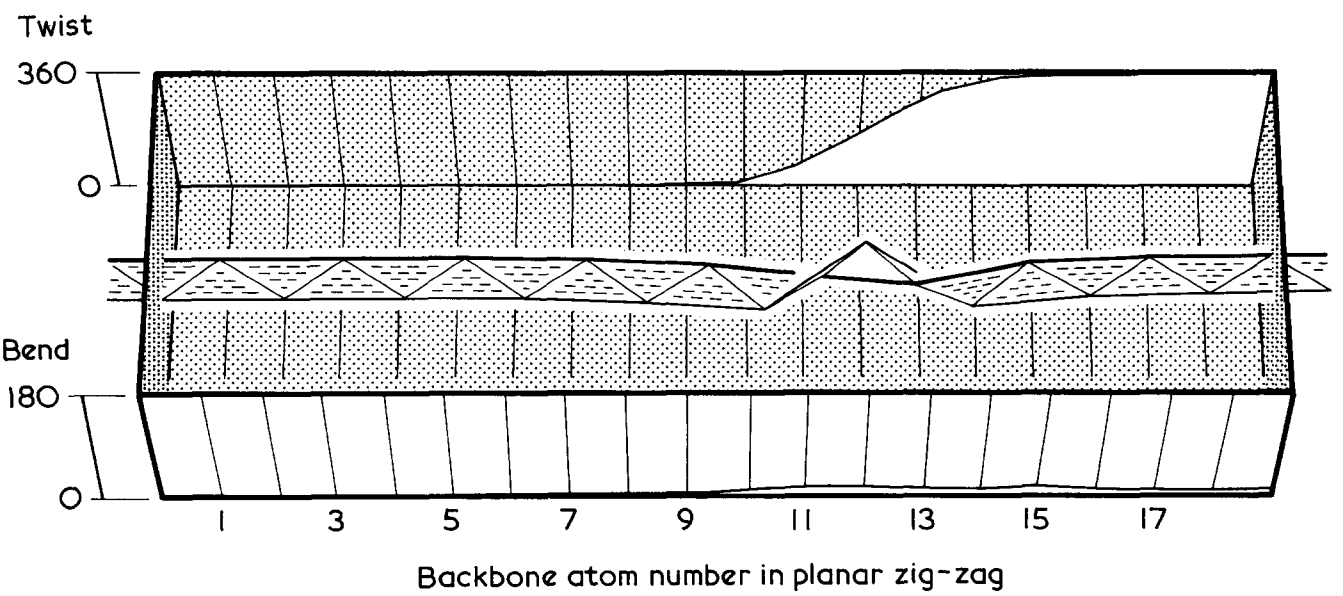

Figure 1 Minimum energy conformation of a disclination in a C-19 oligomer. The two chain ends are not constrained and the chain is slightly contracted, resulting in crystallographic mismatch. Notice that the total 360° twist is almost entirely confined within a 6-bond-long segment. The twist along the chain length is plotted on one side of the box. On the opposite face of the box the accumulated bend is plotted vs. the chain length. When the two ends of the chain are fixed to lattice sites, the twist is more spread out over the chain length, as can be seen from Figures 14A and 14B of ref. 1

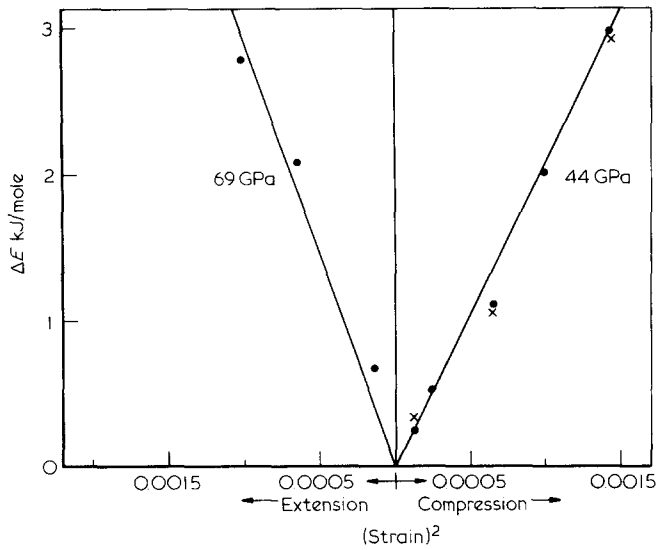

Figure 2 Plot of energy increment *versus* squared strain. Plots are for both contractile and tensile forces. The calculations are on chains of C-15 and C-21 chains containing dispirations. The deformed chains are imbedded in an orthorhombic crystal lattice. The entire system, consisting of the deformed chain and the six chains of the inner shell, was energy-minimized at each step. Calculations were performed at strain intervals of 0.0067. (●) C_{21}; (×) C_{15}

obtained. Since the starting dislocation was not at its minimum energy conformation, normal mode calculations could not be performed for the dislocation.

(b) Calculation of static modulus

The results of the calculations are shown in *Figure 2* and *3*. In these Figures ΔE, energy increments, are plotted *versus* squared strain. The slopes in the linear part of the curves determine the static modulus for the defect. As seen from these Figures, the calculated moduli for tensile and contractile forces are not the same. This difference is associated with the tendency for the defect-containing oligomer to change its overall length as compared with the lengths of the surrounding chains. The resulting apparent asymmetry in the calculated potential is attributed to the fact that the true minimum conformation is not always obtainable with the numerical algorithm employed. This results in the differences in the computed moduli in the shorter chain. In the case of dispiration, the modulus for applied tensile forces is higher, by about 25%, than that computed for contractile applied forces (see *Figure 2*). For tensile forces the modulus for the disclination is lower, and for dislocation higher, than their respective moduli for the contractile forces. We also performed static calculations on shorter chains, with 15 carbon atoms. The modulus could be calculated only for compressive forces because the calculation for tensile forces became numerically unstable. The calculated modulus for a dispiration in a 15 carbon atom oligomer was found to be about 30% lower than that for 21 carbon atom oligomer. Although the exact modulus depends on the detailed structure of the defect, the modulus for all the defects calculated falls in the range of 45 ± 15 GPa.

(c) Defect atom displacements in static calculations

Figure 4 shows the static displacements of chain atoms when a dispiration is subjected to external forces acting along the chain axis in either opposite directions (tensile forces) or toward the molecular centre (contractile forces). The cartesian coordinates employed here are the same as used previously[1]. The z direction coincides with the chain axis. The x direction is perpendicular to the chain axis in the zigzag plane, while the y direction is perpendicular to this plane. The two drawings at the left side and at the right side of *Figure 4* are stereo pairs. In these stereo pairs, the thick line shows displacements for tensile forces, while the thin line describes the case of contractile forces. The overall separation of the terminal atoms was shortened by 0.03 nm for contractile forces, while for tensile forces it was increased by the same amount. *Figure 4* also shows the displacements of the carbon atoms along each of the three cartesian coordinates. There are two sets of these three displacements, one for tensile forces, the other for contractile forces. These displacements are inserted in *Figure 4* between the two stereo pairs. The cartesian displacements are plotted in this Figure *versus* the location of the backbone atoms along the chain axis. The backbone atoms subject to the application of the tensile or contractile forces, and the direction of these forces, are shown by arrows. Particular attention should be given to the transverse displacements shown in *Figure 4*. The significance of these displacements for the problem of defect coupling with the displacements of atoms in the zigzag segments is briefly discussed in Chapter V.

II. NORMAL MODE CALCULATIONS OF THE LOWEST LONGITUDINAL FREQUENCY OF DEFECTS AND INTERRELATION WITH THE RESULTS FROM STATIC CALCULATIONS

The static computations described above provide an estimate of the effective modulus of the defect that, combined with the mass per unit length of the defect, permits the calculation of the lowest longitudinal frequency of the defect. This frequency is associated with a vibration in which the longest dimension of the defect is approximately one-half the wavelength. In a defect there are also frequencies, not discussed in detail in this paper, which are associated with torsional or shear displacements and which are lower in frequency than the lowest longitudinal frequency. The defects are thought of as small resonators with natural frequencies which permit strong interactions with particular normal modes of polyethylene crystals. The normal modes were investi-

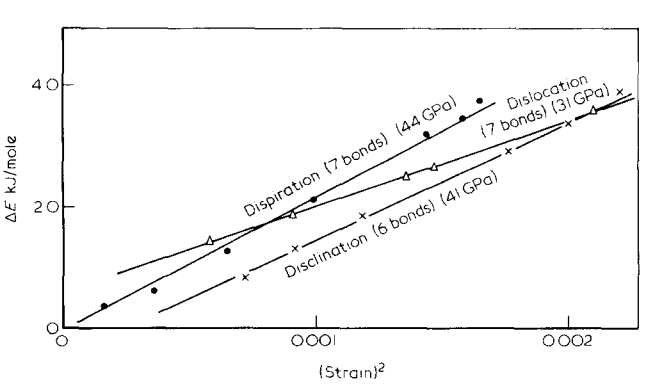

Figure 3 Plot of energy increment *versus* squared strain. The curves compare moduli for the three crystallographic defects of a single chain investigated in the paper, that is, dispiration, disclination, and dislocation. The defect-containing chains are 21 C-atoms long. Calculations are for contractile forces only

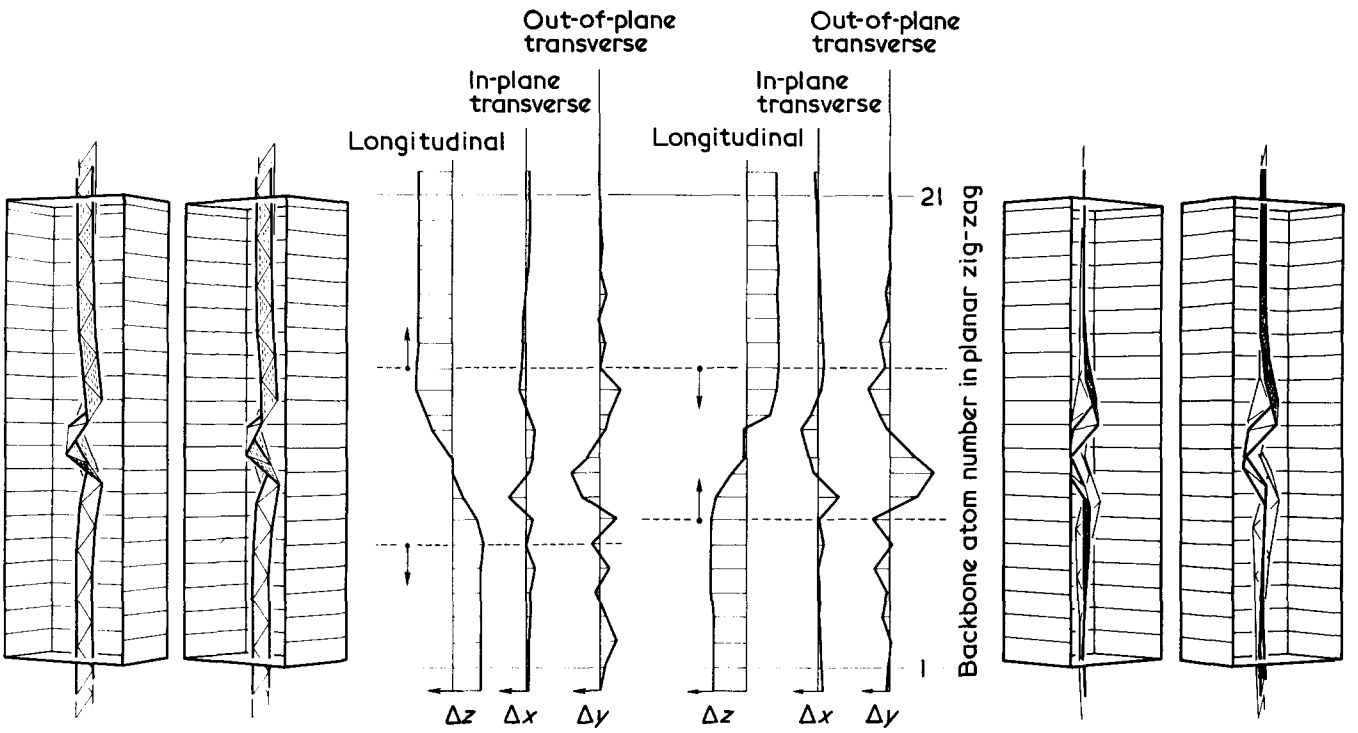

Figure 4 Dispiration near the centre of the C-21 oligomer. Static calculations. The two stereo pairs at the left side and the right side of the Figure show the displacements for tensile forces and for contractile forces superimposed on each other. The thick line is for tensile forces and the thin for contractile forces. The centre of the Figure shows two sets of displacement along the three cartesian axes, one for tensile forces, the other for contractile forces. The atoms initially displaced, and the direction of the displacements are shown by arrows. Notice slight displacements in the transverse (x and y) directions in the zigzag segments, i.e., outside the parts of the chain between the arrows. These displacements result from the motions of the entire chain in the matrix of intermolecular forces

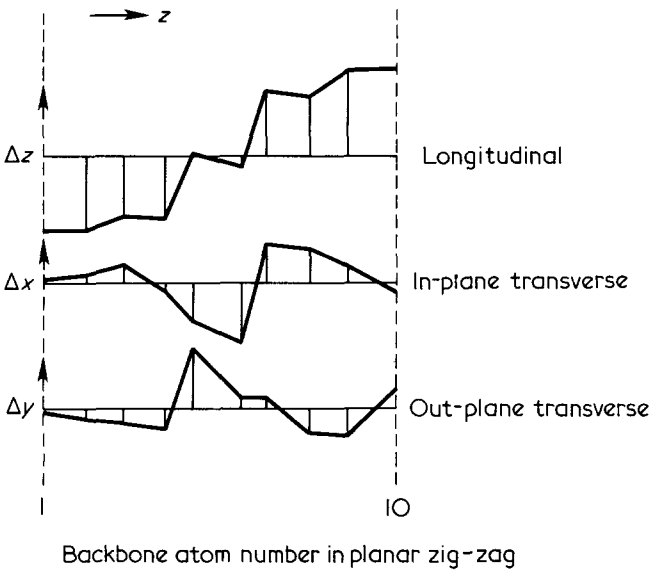

Figure 5 Dispiration in the C-10 chain. Dynamic calculations. Displacements are for the normal frequency of 150 cm^{-1}. The defect is considered to be isolated, i.e., uncoupled to zigzag segments. Notice the longitudinal mode along the chain (z) axis

gated in detail by complete normal mode calculations on oligomer chains containing particular defects in their low-energy conformation at particular points in the chain. In these short oligomers, end effects play a much larger role than in stems of the length found in polyethylene. Effort is required to sort out the features most important in real polyethylene crystals with long planar zigzag segments.

As a first step, normal mode calculations were performed in a lattice built of short chains in which a defect occupies almost the entire length of the central chain. We selected a $C_{10}H_{22}$ oligomer containing a dispiration. The short chain length leaves only the two terminal methyl groups outside the defect. We define this as a bare defect, that is, a defect unperturbed by zigzag segments. The displacements of this defect in the longitudinal (z) direction form a monotonic curve when plotted *versus* the chain-length, as can be seen from *Figure 5*. The displacements associated with this frequency strongly resemble those of LAM-1 in a zigzag chain, except for the presence of a considerable amount of transverse displacement (see *Figure 5*). This is the frequency referred to above as the 'lowest longitudinal frequency of the defect'. The longitudinal displacements with only one node also strongly resemble those of a one-dimensional rod with a mass-per-unit length proportional to N/l, where N is the number of carbon atoms in the defect and l is the length of the defect. In this bare defect, there is a standing wave of wavelength equal to twice the length of the oligomer and with wavenumber $k_z=\pi/l$. This standing wave has displacements similar to these shown in *Figure 4*.

The wavenumber (which is referred to as 'frequency' as is the practice in vibrational spectroscopy) of the defect calculated from the static modulus and the defect length can be approximated from the rod model. The lowest longitudinal frequency of a continuous elastic rod is given by $\nu_{rod}=\frac{1}{2c'L}\sqrt{\frac{G}{\rho}}$ where G is the elastic modulus equal to 44 GPa from *Figure 3*, ρ the density, c' the velocity of light, and L the length of the rod. For both the dispiration and the disclination, $L\cong 0.76$ nm. The predicted defect frequency calculated from the modulus and the length of the defect-rod is found to equal

147 cm^{-1}. This is in a good agreement with the longitudinal frequency of the defect in a 10-carbon atom chain, which is found to equal 150 cm^{-1}. There is an alternative way to estimate the longitudinal frequency of the defect. The observed LAM-1 frequency in crystalline n-heptane, the oligomer whose length is the same as the length of the disclination or dispiration, is 311 cm^{-1}. One has to realize that the rod model is very approximate for short chain oligomers. The calculated frequency for C_7 would be 345 cm^{-1} rather than the observed 311 cm^{-1}. From the ratio of the zigzag modulus to the defect modulus ($340 \div 44 = 7.7$) the predicted longitudinal frequency of the defect is 125 cm^{-1}, again in qualitative agreement with our estimate based on the calculations for a defect in a C-10 oligomer.

When the ends of a defect are both coupled to zigzag segments, the basic features of the defect vibration described above are preserved. The coupling of the defect to zigzag segments tends to lower the frequency of the defect. In short chains the defect frequency decreases with the increase in the length of the zigzag segment coupled to it, and rapidly reaches a limiting value, as the zigzag segment length increases. In the C-15 oligomer, the longitudinal frequency of the defect in our crystal model is split into three frequencies, 121, 107 and 90 cm^{-1}. In C-21 oligomer, the defect frequencies occupy a range between 105 and 85 cm^{-1}. This frequency range is found to be independent of the defect position in the chain, although the exact frequencies are dependent on defect position. The lowering of the defect frequency when it is coupled to zigzag segments can be attributed to a mass effect. The problem of the mass effect on lowering the frequencies has been originally treated by Fanconi and Crissman[10], who investigated the effect of a methyl group branch on the LAM-1 frequency in a zigzag chain. The point mass required to create the calculated frequency lowering can be estimated from the mass perturbation theory of Hsu and Krimm[11]. The added effective mass required at each end of a defect is found to be only 18 to 20 atomic mass units, hardly exceeding the mass of a methylene group. Considering the fact that the effective mass of the defect-resonator is rather small, the coupling of the defect to the zigzag segments can easily account for the observed decrease in its frequency. The existence of a longitudinal frequency for a defect, that is a frequency which is independent of the length of attached chains, can also be inferred from a study of the relaxation and correlation of the motion of two heavy masses separated by a finite number of particles with small masses, all of them coupled by harmonic forces to their neighbours in an infinitely long chain[12]. In a related problem, the effect of nonplanar zigzag sequences on the frequency of the unperturbed longitudinal acoustic mode was investigated theoretically by Strobl[13].

III. ANALYSIS OF NORMAL MODE CALCULATIONS

In this work we are concerned only with those dispersion curves that correspond to the low-frequency vibrations of the crystal. Although commonly referred to as curves, the dispersion relations for a crystal are a set of sheets in a 4-dimensional space which show the eigen-frequencies of the crystal for each crystal momentum vector $\underline{k}$ in reciprocal lattice space (also called momentum space or phase space). For polymer crystals an interesting part of the dispersion relations corresponds to waves propagating along the chain or z-axis. Plotted as frequency *versus* phase, those are the curves that spectroscopists often use to summarize their comparisons of experimental and calculated frequencies. We will use them to analyse the coupling between defect and lattice vibrations. After a discussion of dispersion curves for waves propagating in the chain direction in various models and crystallographic modifications of polyethylene, we will comment on the coupling between defect vibrations and waves propagating in other directions through the crystal, using the information available in literature.

(a) *Low frequency dispersion curves for oligomer crystal model used for defect energy calculations*

Our normal coordinate calculation for a defect-containing lattice are based on a model which assumes that the neighbours to the defect-containing chain are deformed to minimize energy but do not vibrate. In order to gain insight into the nature of coupling of the vibrating defect with the zigzag chain segments, a dispersion curve for a central molecule in the planar zigzag conformation in which the chains surrounding the central, vibrating chain are kept rigid, was calculated, and is

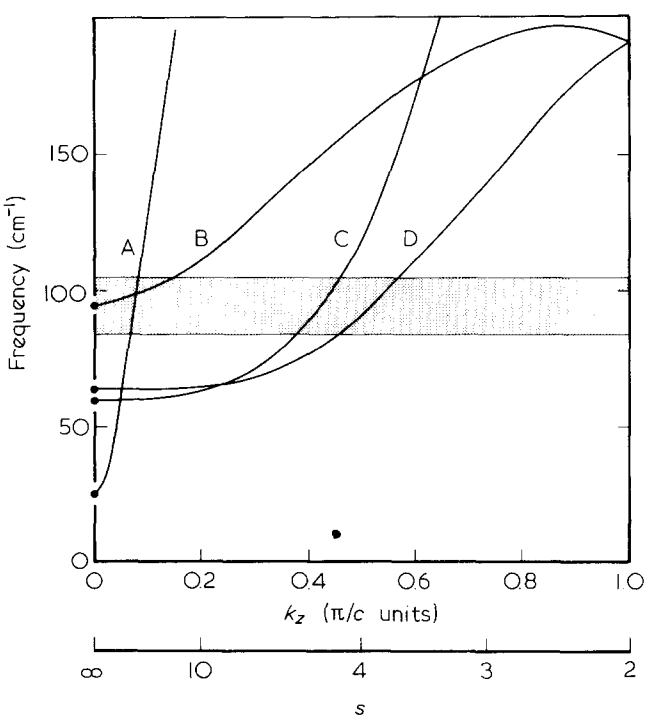

Figure 6 Low frequency dispersion curves showing coupling of defect vibrations to points on the dispersion curves. The basis for the calculated frequency *versus* wave vector curves is the lattice model employed in the present work. The four branches of the dispersion curves are labelled A, B, C and D. The shaded area shows the frequency range at which the frequencies of the vibrating zigzag segments are in the range of the lowest longitudinal frequency of a defect. The frequencies are plotted *versus* k_z, the component of the wave vector along the z axis, assuming that the components of the vector $\underline{k}$ in directions perpendicular to the chain axis are zero. In this Figure and the subsequent two dispersion curves k_z is in π/c units with $c = 0.247$ nm. The bottom scale of the abscissa is in terms of s, the number of C–C bonds between nodes. The relationship between k_z and s is given in the text

shown in *Figure 6*. The dispersion curves shown in *Figure 6* were calculated on the basis of normal coordinate calculations performed on series of crystalline n-alkanes (C-7 to C-21). The dispersion curves were extrapolated to the wavevector $\underline{k}=0$. In *Figure 6* the components of the wavevector $\underline{k}$ in directions perpendicular to the chain axis are zero. Hence, $\underline{k}=k_z$, and k_z ranges from 0 to k_z max, which is π/c ($c=0.247$ nm, the crystallographic repeat distance). The calculated dispersion curves are shown for the first Brillouin zone for the unit cell with a repeat unit of two CH_2 groups.

Spectroscopists customarily replace the momentum vector $\underline{k}$ by the dimensionless phase difference vector ϕ. The domain of this vector is called phase difference space. The allowed values of this vector are in a cell with origin at (0,0,0) and other corners located at (α,β,γ) where α, β and γ assume either 0 or π values. In *Figure 6*, the dispersion curves are plotted *versus* the phase differences along the z-axis, that is, versus k_z in units of π/c. There are four separate dispersion curves which are monotonic functions of frequency in the low frequency range of interest, i.e., in the range of the calculated defect frequencies. These curves, referred to as branches of a multivalued function of frequency as a function of the wave vector $\underline{k}$, are marked by A, B, C and D in *Figure 6*. The zero wave vector frequencies of the modes observable in Raman and infra-red spectroscopy are indicated by the $k_z=0$ intercepts of the four branches with the frequency axis. Normal coordinate analysis assigns the frequency at the intersection of the B branch with the frequency axis of *Figure 6* to twisting oscillations of the chain about its longitudinal axis (also called the optical rotational mode in the polymer literature). The remaining three branches intersect the $k_z=0$ axis at frequencies of an undeformable rod vibrating in an anisotropic elastic matrix. In an infinite lattice, these frequencies are zero, as they correspond to chain translations. The frequencies of branch A are those of an elastic rod vibrating with displacements only along its axis (often called the longitudinal acoustic mode in polymer literature), while the points on branches C and D at $k_z=0$ are for an elastic rod vibrating with displacements in the two orthogonal directions perpendicular to the chain axis (transverse acoustic modes).

(b) Coupling of defect mode to zigzag segments—general considerations

In order to gain insight into the nature of the vibrational coupling between a defect and the adjoining zigzag segments, the computed displacement amplitudes, or eigenvectors, are presented in the cartesian coordinate system described in the section on static calculations. The advantage of this coordinate system results from the characteristics of the dispersion curve for an isolated chain. In an isolated chain, branches B and D are dispersion curves for the out-of-plane vibrations. The branch B is recognized as twisting mode and the branch D as an out-of-plane bending mode[14]. In an isolated chain these branches are recognized as torsional or out-of-plane transverse acoustical modes. Moreover, in the frequency region of interest here, branch A represents displacements which are almost entirely longitudinal, and branch C, transverse in-plane bending vibrations. Those characteristics of the isolated chain model are largely preserved in the lattice model employed here, except near $\underline{k}=(0,0,0)$. The displacements of the modes with which a defect can couple at the natural frequency are then: longitudinal (Δz), in-plane (Δx), and out-of-plane (Δy) transverse modes.

It is of some interest to compare the defect-associated modes with the modes of a planar zigzag molecule, but the usual terminology of spectroscopy is inadequate to describe the defect-associated displacements. Computer graphics displays now make it feasible to observe the displacements in a movie-like display, and in the stereographic views presented in this paper.

The dispersion curves in *Figure 6* are also plotted *versus* s, the number of C–C bonds between adjacent nodes. For the branches A, B, C and D the relationship between s and k_z is as follows. If λ is a wavelength and the crystallographic repeat unit c is two CH_2 groups, then $\lambda=2\pi/k_z$ and $s=\lambda/c$. Branch B is different in that the displacements Δy of two adjacent C atoms are generally of opposite sign. This means that each segment of the chain is rotating and in general the chain segments twist and untwist. This description conforms to the conventional designation of this branch as displaying a chain twist mode in the isolated chain model and s is a measure of the distance between nodes in the amount of twist.

In *Figure 6*, the shading covers the part of the dispersion curves for which the corresponding frequencies are within the range that can couple to the lowest longitudinal frequency of the defect. The range of the possible values of the parameter s for each of the four branches within this frequency range is shown in *Figure 6*. *Table 1* tabulates the range of s for the four branches.

The coupling of the defect oscillator to the zigzag segments has been analysed only for relatively short oligomer chains, because the cost of the calculations grows rapidly with the chain length. The behaviour of long chains can be deduced from the oligomer calculations with the aid of dispersion curves for polyethylene shown in *Figure 6*. For the branches C and D, the parameter s which measures the half wavelength in the vibrating zigzag segment coupled to the defect, is sufficiently small (see also *Table 2*) so that the modes associated with branches C and D are easily observed in the systems calculated here. For the branches A and B, s is large and the modes associated with these branches are affected by the shortness of the oligomers. Coupling to branch B is observed in short chains, by noticing the tendency of the bonded C atoms to have displacements of opposite sense, that is a tendency for the chain to rotate or twist. The dispersion curve leads to an estimate of s for the frequency of 100 cm^{-1}, at which coupling of defect to the branch B is observed (see *Figure 6*) as about 12. The observed value of s (see *Figure 9* below) is about 6. This discrepancy could be attributed to the relative flatness of the B branch at low values of k_z and to difficulty in correctly assessing the wavelength of the vibrating zigzag segment from the data based on short chains. Coupling to branch A cannot be observed in short chains. For the branch A, s is around 20–30 and the longitudinal half

Table 1 Ranges of expected values of s for the four branches of *Figure 6*, in the frequency range shown by the shaded part

Branch	A	B	C	D
s	22–29	12–∞	4.2–5.2	3.6–4.3

Table 2 Coupling of defect to zigzag segments at the lowest longitudinal frequency of defects. Comparison of data from disposition curves with the data from the computed Eigenvectors

Model	ν (cm^{-1})	$k_z \cdot 10^8$ (cm^{-1})	s	Branch of dispersion curves (see *Figure 7*) at coupling point	s, (from displacement figures)	Frequencies, in cm^{-1}, of zigzag C'_{21} with nearest s
Dispiration near	100	0.12	1.0	B	1.0	100 (s=1)
chain end of C_{21}	87	0.59	4.2	D	4.4	89 (s=4)
	84	0.47	5.2	C	6.0	86 (s=0)
Dispiration near	106	0.68	3.6	D	4.0	107 (s=3); 89 (s=4)
centre of C_{21}	99	0.55	4.5	C	4.5	118 (s=4)
		0.68	3.6	D	3.5	107 (s=3) [a]
	93	0.00	1.0	B	1.0	97 (s=1)
		0.52	4.8	C	5.0	86 (s=5)
Disclination in C_{21}	94	0.53	4.7	C	5.0	86 (s=5)
		0.64	3.9	D	4.0	89 (s=4)
	69	0.37	6.7	C	6.5	65 (s=6)
		0.42	5.9	D	5.2	75 (s=5)

[a] One zigzag segment vibrates with almost equal displacements in two transverse direction. Behaviour of longer chains cannot be assessed

wavelength is about 5 nm, a condition easily met in a real crystal, but not met in calculations for the short chains described in this work.

(c) Defect mode coupling to zigzag segments from normal mode calculations

In addition to the coupling of a defect with points on several different dispersion curves, the stems at opposite ends of the defect can also vibrate simultaneously in several modes associated with the same dispersion curve if the defect natural frequency is near a flat part of a dispersion curve or if the stem is very long so that allowed frequencies are closely spaced. For example, for a dispiration near the chain end, two modes coupling with the branch B are observed in computations, one at 100 cm^{-1}, the other at 97 cm^{-1} (see also *Figure 6* and *Table 2*). An example of a disclination that couples to two rather widely spaced frequencies will be discussed in more detail below. It will be shown that this large frequency split is a direct consequence of the shortness of the chain containing the defect.

Figures 7–9 show typical low-frequency displacements of atoms for a chain which contains a defect in a crystal. The modes shown were selected to show displacements which are associated with each of the three branches, B, C and D, shown in *Figure 6*. The part of the vibrating zigzag segment which is about one wavelength from the defect shows the characteristic displacements of the modes best. While the part of the zigzag segment near the defect shows a mixture of modes, ultimately the zigzag segment farther away from the defect must vibrate with displacement vectors characteristic of lattice vibrations. The dispiration located near the end of the C-21 oligomer provides the best examples, as the attached zigzag segment is as long as possible. The general description given for *Figure 4* also applied to these Figures. The coordinate system in *Figures 7–9* is the same as that employed with the static calculations. The two drawings at the left side and the two drawings at the right side are stereo pairs showing the displacements. The displacements shown are superpositions of two displacements, one at phase angle 0, the other one at phase 180°. All the displacements shown in the Figures were obtained by multiplying the orthonormalized displacement eigenvectors by a constant, here 0.3 nm. The real displacements are too small to be seen in these drawings. For example at room temperature, the estimated longitudinal amplitudes of the terminal atoms do not exceed 0.006 nm. The graphs inserted between the two stereo parts in each one of the *Figures 7–9* show the components of the displacement of each atom along the three cartesian coordinates.

Figure 7, for $\nu = 87$ cm^{-1}, shows the defect coupled with a zigzag segment vibrating with out-of-plane bending displacements, associated with a point on the branch D. This Figure shows a small amount of twist near the defect. *Figure 8*, for $\nu = 84$ cm^{-1}, shows that the in-plane bending (associated with the branch C) is dominant. There is again a small amount of twist close to the defect. *Figure 9*, for $\nu = 100$ cm^{-1}, shows that the zigzag segment twists, i.e., the zigzag vibrates with displacements associated with the branch B. There is a small amount of in-plane and out-of-plane bending in the zigzag segment displacements. All three Figures also show modest longitudinal displacements, which suggest that in a longer stem there would be coupling to a longitudinal acoustic mode of wavelength too long to be encompassed by our calculations on C-21 oligomers. The longitudinal displacements are more dominant in *Figure 9* than in *Figures 7* and *8*. The particular mode displayed by this Figure has the highest Raman intensity associated with this particular defect model and the position it occupies in the C-21 oligomer (see also *Table 3* below). The LAM-1 like displacements provide the dominant part of the contribution of the defect itself toward the calculated Raman intensity. In long chains the presence of LAM displacements outside the defect could also affect the total Raman intensity for the particular defect mode. Besides the modes displayed in *Figures 7–9*, there are other modes which involve coupling between defects and lattice modes. Some are strongly affected by the chain ends.

The defect modes are summarized in *Table 2*. The guideline for inclusion of a particular mode in this Table is the presence of distinct longitudinal displacements plus a significant calculated Raman intensity. Column 1 of this Table describes the kind and position of a defect in a C-21 chain. Column 2 gives the frequency of the defect mode, i.e., the frequency of the defect coupled to the model crystal. In columns 3–5 we present data calculated from the dispersion curves shown in *Figure 6* and *Table 1*. These are: k_z, the component of the wave vector along the chain axis (column 3); s, the number of C–C bonds between nodes in the vibrating segment (column 4);

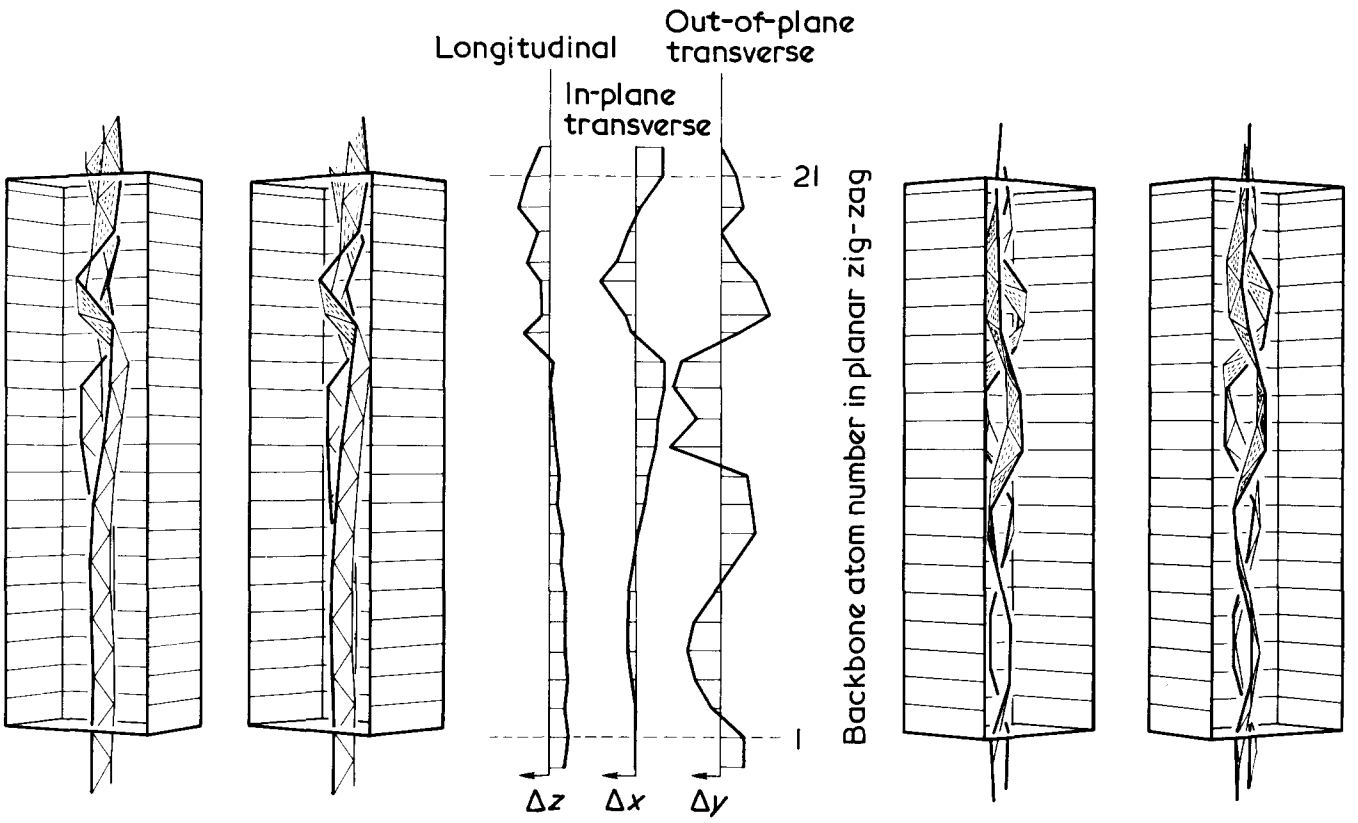

Figure 7 Dispiration defect near the upper end of the C-21 oligomer. Displacements are for the normal mode at 87 cm^{-1}. The zigzag segment vibrates with transverse displacements predominantly in the *y* direction, associated with a point on the dispersion curve D. The central part of this Figure shows the components of the displacement at each carbon atom. The stereographic pair at the left shows the vibrating chain viewed along a direction nearly perpendicular to the zigzag plane. At the right the view direction is nearly in the plane of the zigzag and the out of plane (Δy) displacements are clearly evident. Each of the stereographic pairs shows both the positive and negative displacements. *Figures 8* and *9* are arranged in a similar way

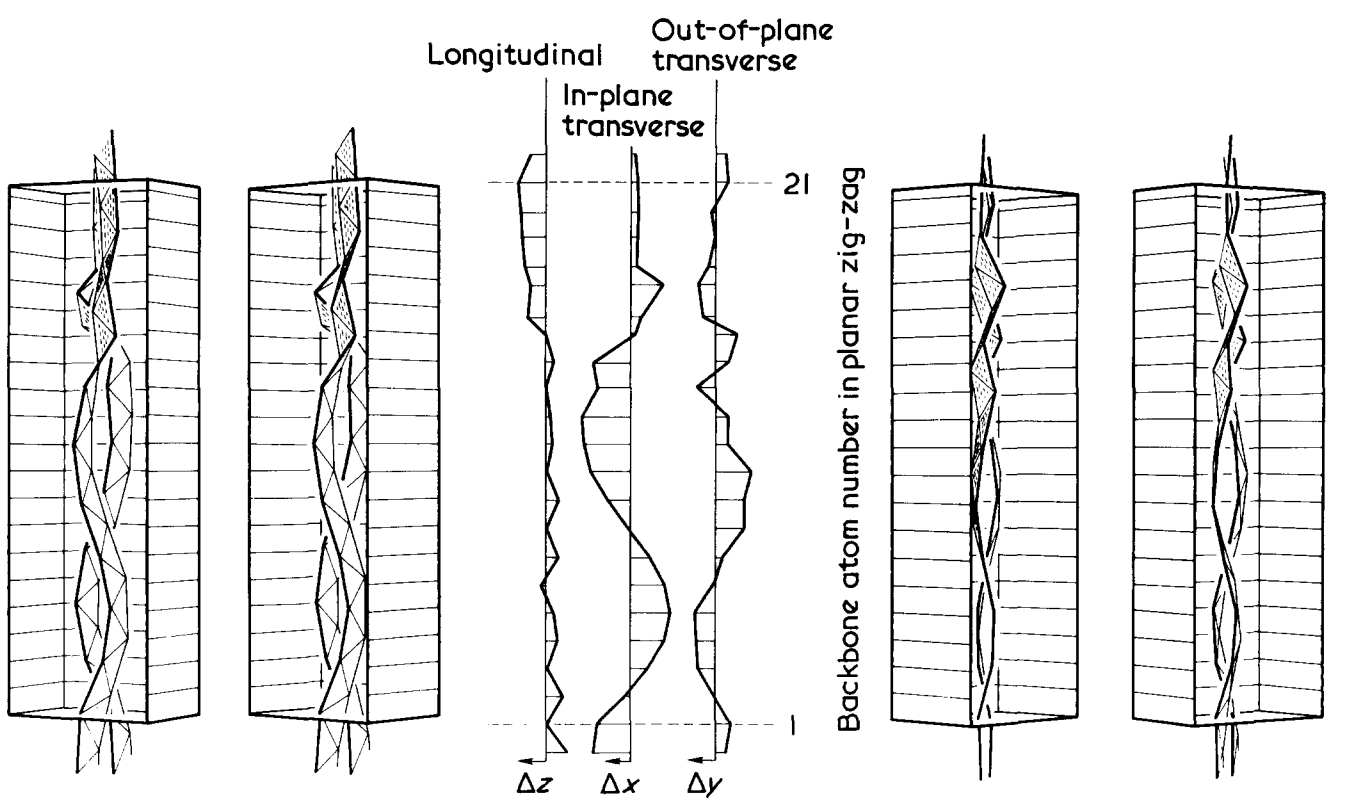

Figure 8 Dispiration near the end of the C-21 oligomer. Displacements are for the normal mode at 84 cm^{-1}. The zigzag segment vibrates with transverse displacements predominantly in the *x* direction, associated with a point on the dispersion curve C

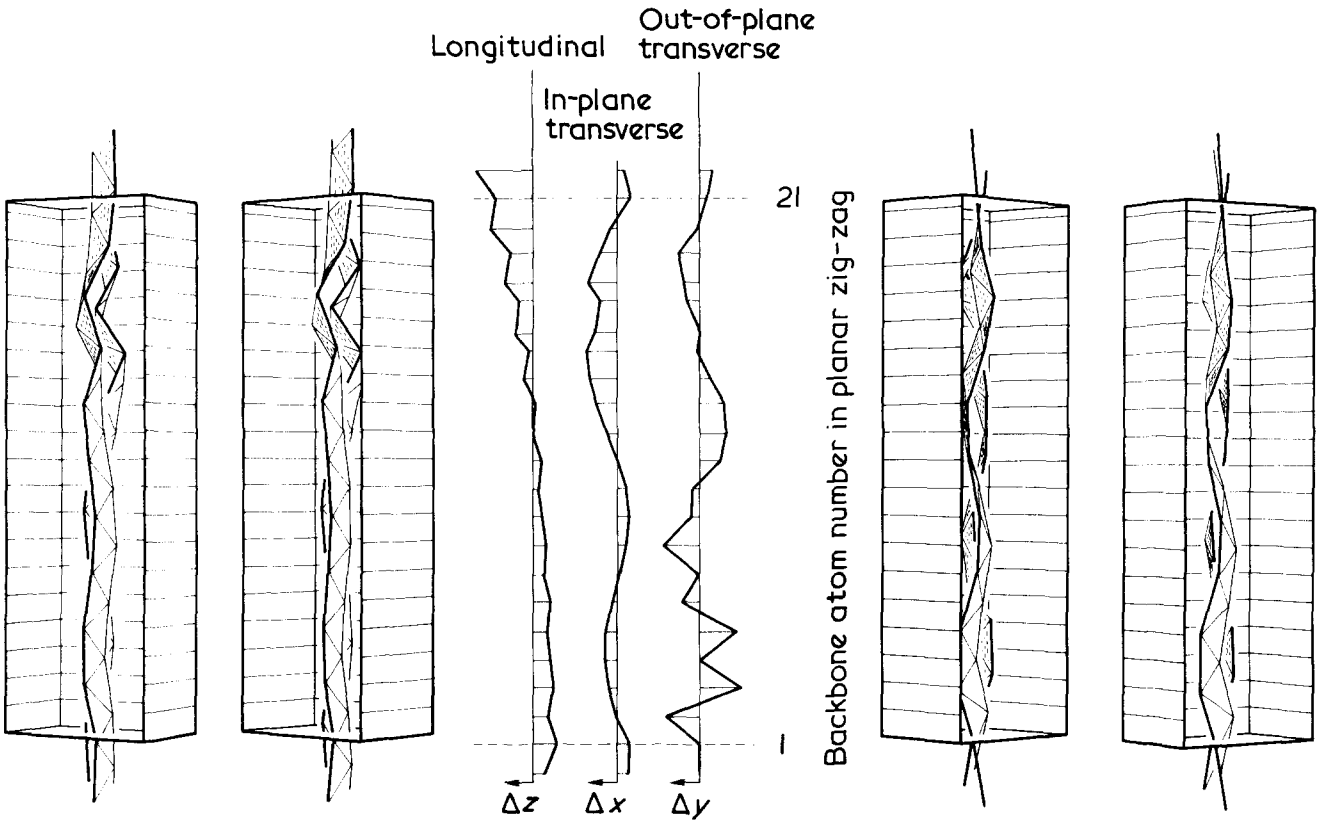

Figure 9 Dispiration defect near the upper end of the C-21 oligomer. Displacements are for the normal mode at 100 cm^{-1}. The zigzag segment twists, that is, it vibrates as an optical wave with displacements predominantly in the *y* direction, associated with a point on the dispersion curve B

Table 3 Raman intensities attributed to defect oscillators

Model	*N*	ν_k (in cm^{-1})	α'^2	$\Sigma \nu^{-1} \alpha'^2 \times 10^4$ [a] $k\ k\ k$	$I/I_{Lam-1,zigzag}$ [b]
Dispiration	10	151	0.0139	0.921	0.161
Dispiration	15	119	0.0123	1.216	0.136
		110	0.0020		0.022
Dispiration near end	21	100	0.0109		0.152
		87	0.0059	2.004	0.083
		84	0.0024		0.064
Dispiration near centre	21	99	0.0071		0.105
		93	0.0061	1.713	0.092
		88	0.0030		0.051
Disclination near centre	21	94	0.0044	0.917	0.063
		69	0.0031		0.064

[a]
$$I_{\text{Raman},k} = \frac{(\nu_k - \nu_0)^4 \bar{\alpha}_k'^2}{\nu_k(1 - e^{-hc\nu_k/kT})} \propto \frac{\bar{\alpha}_k'^2}{\nu_k}$$

[b]
$$\frac{I_k}{I_{\text{Lam}-1}} = \frac{\bar{\alpha}_k'^2}{\alpha_{\text{Lam}-1}'^2} \cdot \frac{\nu_{\text{Lam}-1}}{\nu_k}$$

designation of the particular branch of the set of dispersion curves (column 5). In column 6 the parameter *s*, obtained directly from the displacement curves, is presented. As is seen, values of *s* given in columns 4 and 6 agree well. In column 7 an estimate of the frequency of the vibrating zigzag segment coupled to the defect is given for each of the cases described in this Table. This estimate is based on the independent computations of normal modes performed on a system built entirely of C-21 zigzag chains, with only the central chain vibrating. Each frequency in column 7 is accompanied, in parentheses, by a value of *s* defined here as (20)/(number of nodes). The number of nodes were calculated directly from the normal coordinate analysis performed on the C-21 oligomer in the

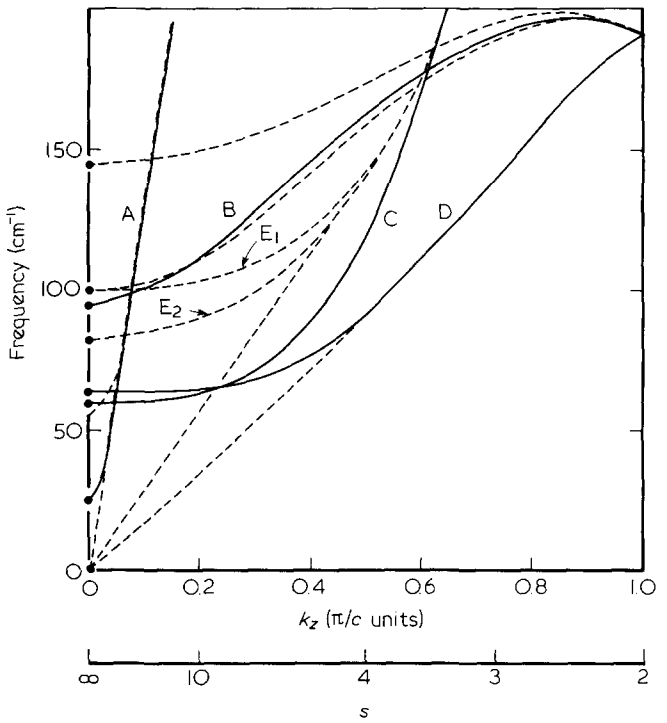

Figure 10 Comparison of dispersion curves based on the model used for calculations (solid lines) with the dispersion curves for the orthorhombic lattice (broken lines). The four dispersion curves based on the model are marked by the letters A, B, C and D

zigzag conformation.

The displacements for a disclination at the two frequencies of 94 and 69 cm^{-1} (last two lines in *Table 2*) show an interesting feature. The modes at these frequencies both show coupling with branch C at one side of the defect and branch D at the other side. The wavelengths of the two vibrating zigzag segments (C and D) at the lower frequency are longer than they are at the higher frequency as measured by an increase in the parameter s by 1, that is, the wavelength at the lower frequency is incremented by the length of one C–C bond (see *Table 2*). We explain the rather large frequency split by perturbation of the vibrational energy levels created by chain-end effects. Application of the first order perturbation theory to the lowest longitudinal frequency of the disclination predicts that this frequency will be shifted by equal amounts up and down from the unperturbed defect frequency, which is calculated as equal 82 cm^{-1}. Mathematically, there are two degenerate unperturbed defect frequencies, which are very close and which tend to separate as the result of the perturbation interactions. The frequency shift can be associated with the perturbation function W which represents the chain-end effects. W decreases with the increase in the chain length. This decrease of W was also confirmed in ref. 15, where the perturbation effects were related to the mass differences between the terminal methyl groups and the methylene groups in crystalline n-alkanes. Thus, the rather large frequency difference between the two disclination modes is considered to be an artifact of the system built of short oligomers.

In this paper, we are primarily concerned with the coupling to zigzag segments at the lowest longitudinal frequency of a defect. At this frequency, the wavelength is approximately equal to twice the length of the defect. A bare defect displays other longitudinal modes. One mode, at $\nu = 395$ cm^{-1}, has a wavelength equal to the length of the defect; another mode at $\nu = 518$ cm^{-1}, has a wavelength equal to 2/3 the defect length.

As was the situation with the lowest longitudinal frequency of the defect, attaching a stem to a defect lowers the frequency of the higher order modes of the defect. At the frequency of the higher order modes only branches A and C provide lattice modes to which the defects can couple. These have sufficiently low values of s and were clearly observed in plots of displacements (not presented in this paper).

IV. GENERAL ANALYSIS OF DEFECT COUPLING TO LATTICE VIBRATIONS

(a) *Phonons propagating in the chain direction*

Although the dispersion curves associated with the model used in our calculations demonstrate the general features of the coupling of defect and lattice vibrations, more realistic dispersion curves have been determined for polyethylene. Examination of these curves reveals the possibility of additional ways that defect and lattice vibrations can be coupled.

In *Figures 10* and *11*, the dispersion curves of *Figure 6* are plotted alongside the similar dispersion curves for the orthorhombic lattice (*Figure 10*) and the triclinic lattice (*Figure 11*) of polyethylene. The data for these curves are adapted from the literature[6], to correspond to the first Brillouin zone. In an orthorhombic lattice, there are four additional branches (all optical) of the dispersion curves in the frequency region of interest. This is a consequence of having two chains in the Bravais unit cell. The number of different branches to which a defect in a real crystal can couple is greater in an orthorhombic lattice than it is in the lattice model employed in this work or in the triclinic

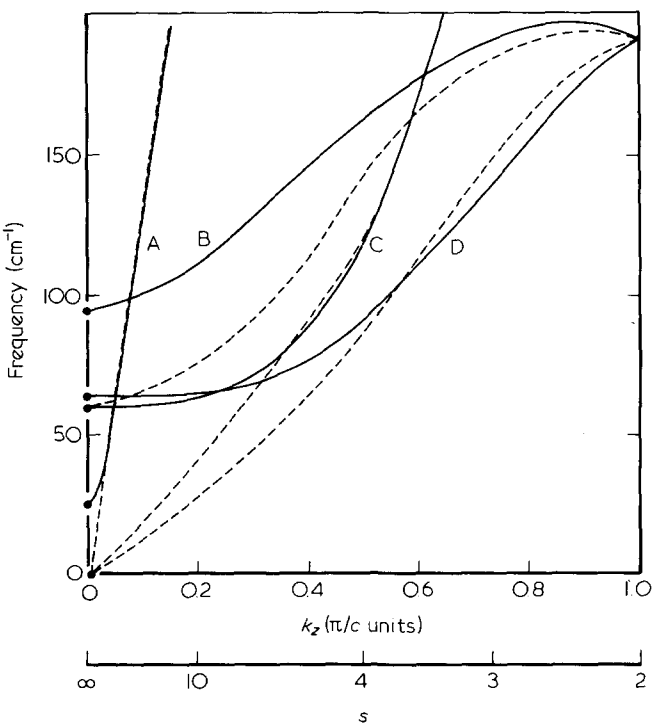

Figure 11 Comparison of dispersion curves based on the lattice model used for calculations (solid lines) with the dispersion curves for the triclinic lattice (broken lines). The four dispersion curves based on the model are marked by the letters A, B, C and D

lattice. Inspection of *Figure 10* indicates that the coupling of acoustic branches (one longitudinal, equivalent to our branch A, and two transverse, equivalent to our branches C and D) lead to approximately the same set of values of s, the number of C–C bonds between adjacent nodes in displacement curves as found with our lattice model. *Figure 10* shows two branches, whose frequency does not vanish at $\underline{k}=(0,0,0)$ (therefore called 'optical'). One of these two branches, which is a twisting mode, practically coincides with the branch B. The value of s for the defect coupling with this branch is about the same as for the single vibrating chain model used in our calculations. Of the remaining four branches in the orthorhombic lattice, two intersect the frequency range of the lowest longitudinal frequencies of defects. These two transverse branches are designated in *Figure 10* as E_1 and E_2. (In spectroscopy, the frequencies of these branches at the centre of the Brillouin zone are sometimes denoted as B_{1u} and B_{2u}). Since these dispersion curves are rather flat for $0<k_z<0.2\,\pi/c$, showing little frequency dispersion in this region, the corresponding value of s can only be given as an inequality, $s>10$. This indicates long waves.

The calculated dispersion curves for the triclinic lattice (see *Figure 11*) show very close agreement with those for the C-21 oligomer for branches A, C and D for frequencies above 60 cm^{-1}. The values of s for the defect coupled with any one of these branches is therefore the same for both the model employed here and the triclinic lattice. For the branch B, the two models differ considerably.

(b) Phonons propagating in directions transverse to the chain axis

Kitagawa and Miyazawa[7] presented a set of calculated dispersion curves for orthorhombic polyethylene crystals (see ref. 7; Figure V5, a–h). These Figures were examined for possible interactions of the crystal modes represented by the dispersion curves with a defect vibrating at its natural frequency for propagation directions other than the chain axis direction. The Kitagawa and Miyazawa dispersion curves give the frequencies for the wave vectors that terminate on the edges of the reciprocal unit cell. The results of this examination are summarized as follows:

(1) For the $\underline{k}$ vectors which terminate along the three edges of the reciprocal cell that are parallel to the chain axis but do not terminate at the origin, the defect can couple with the same number of branches at the same values of s as was the case for $\underline{k}=(0,0,k_z)$.

(2) The six acoustical branches for $\underline{k}$ transverse to the chain axis in the two orthogonal directions have lower frequencies than is the case with $\underline{k}=(0,0,k_z)$. This is a consequence of the fact that intermolecular forces are much weaker than the forces responsible for the skeletal deformations. Since the lowest longitudinal frequency of the defects is higher than the maximum frequencies of these acoustical modes, no coupling occurs with these acoustic branches. Only one 'optical' branch can interact with the defect. This branch has its maximum frequency at the point $\underline{k}=(0,0,0)$. However, since this maximal frequency associated with this optical branch exceeds, albeit only slightly, the lowest longitudinal frequency of the vibrating defect, coupling to the defect mode can occur. This optical branch shows little dependence on $\underline{k}$ around the frequency of the defect. Hence the value of s at which coupling to the defect can occur is estimated only as an inequality, specifically, $s>6$.

(3) For the $\underline{k}$ vectors with $k_z=0$ which terminate along the edges of the reciprocal cell which do not pass through $\underline{k}=(0,0,0)$, the defect couples with the same number of branches and at the same values of s, as described in (2).

(4) For the $\underline{k}$ vectors which terminate along the edges of the reciprocal cell for which $k_z=\pi/c$, while one of the two other components of the wavevector is varied, the other one assuming either zero or its maximum value, there is no coupling between the lowest longitudinal defect frequency and these dispersion curves. The dispersion curves each have a constant frequency which is either higher or lower than the defect frequency [see also *Figure 10* which shows those frequencies on the $(0,0,\pi/c)$ axis].

V. RAMAN INTENSITIES OF DEFECT OSCILLATORS

The lowest longitudinal frequency of the defect is Raman-active since the asosciated displacements in the longitudinal direction are monotonic functions of position along the chain axis. There are, in our normal mode calculations, frequencies which are lower than the lowest longitudinal natural frequency of the defect. They belong to modes which are predominantly transverse. These frequencies, which occupy a range of 70–60 cm^{-1}, couple with zigzag modes in similar frequency range. These defect modes were found to be practically Raman-inactive. However, they could be infrared-active.

Raman polarizabilities associated with the deformations of the C–C bonds and the C–C–C bond angles can be calculated by a dot product[2], or by a bond polarizability method. The second method is employed here as it yields absolute values of relative intensities. In this method, the cartesian displacements are transformed to displacements (amplitudes) of internal coordinates, via the B matrix transformation, as described in the monograph by Wilson, Decius and Cross[16]. The quantity we calculate is the mean squared polarizability $\alpha_m'^2$, associated with a mode m. Following the method of Mazur and Fanconi[15], the mean polarizability is taken as a sum of the molecular polarizability associated with bond length and the C–C–C bond angle, since the mean derived polarizabilities for the C–C bond and the C–C–C bond angle are assumed to be equal.

In the frequency range of interest, the intensity scattered by the defect oscillator can be assumed to be proportional to the squared mean polarizability of the bonds in the C-21 chain and inversely proportional to the frequency. In this approximation, the temperature effects which enter via the Boltzmann factor in the quantum mechanical expression for the intensity scattered by a molecule, are neglected. In the calculations, all the N bonds and the N-1 skeletal bond angles are included. We also calculated separately the contribution to the Raman intensity from the defect only. It turned out that, for the frequencies associated with the lowest longitudinal defect frequency, the Raman intensity is mostly confined to the defect. However, there is a significant contribution to the Raman intensity from the zigzag segments near the defect. *Table 3* summarizes the results. In this Table, in addition to the calculated squared mean polarizabilities for the entire chain, we also present the ratio of the calculated intensities to those for the LAM-1 mode in a zigzag segment having the same number of carbon atoms as are in the defect-containing oligomer. *Table 3* shows that,

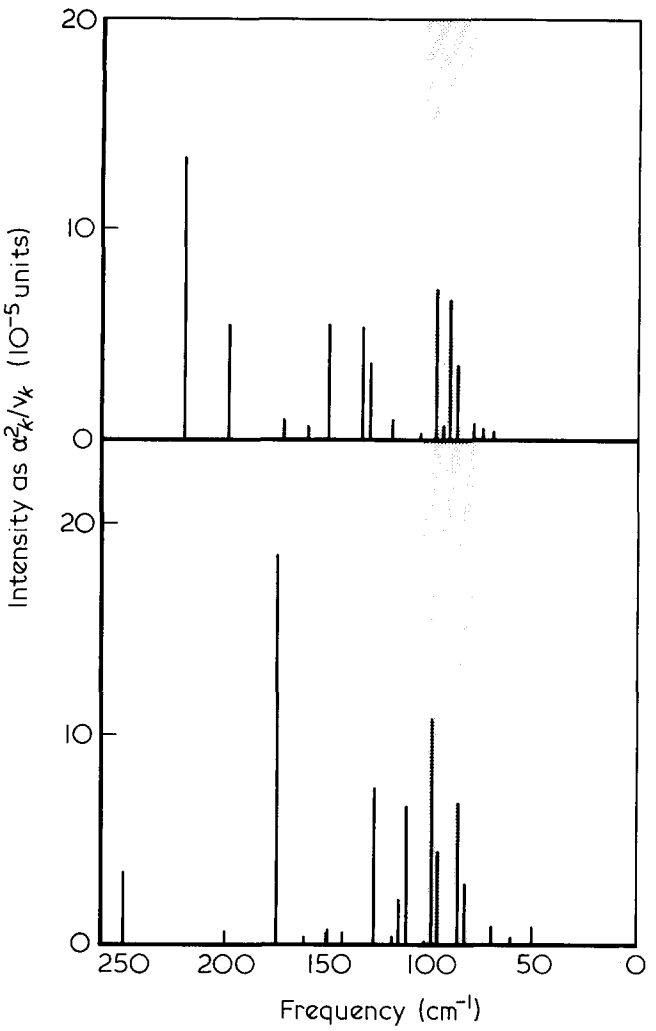

Figure 12 Spectrum for C-21 with a dispiration. Frequency range is 250 cm^{-1} to 0. Top plot: dispiration is located near end of chain. Bottom plot: dispiration is located near middle of chain. The frequency range which includes the intensities attributed to the longitudinal vibrations of the defect are indicated by the shading

approximately, the sum of intensities of all the modes to which a particular defect is coupled tends to be independent of the length of the defect-containing chain. The deviations from a constant sum are attributed to the following chain-length effects: the Raman intensity involves derivatives of the internal coordinates with respect to the position coordinates in the cartesian coordinate system. Small deviations of the positions of the carbon atoms located near the defect from their perfect zigzag conformation can contribute significantly to the mean molecular polarizability and to the related Raman intensity of the chain. In longer zigzag chain segments these effects will tend to be localized, that is, the Raman intensity will be independent of the chain length.

There are other defect modes which are associated with longitudinal wavelengths which are shorter than twice the defect length. These defect modes, by the virtue of their couplings to the higher-order longitudinal modes of the zigzag segments, contribute to the Raman intensities outside the frequency range covered by the *Table 3*. In *Figure 12* we present the intensities, defined as $\alpha_k'^2/\nu_k$ *versus* the frequency. The Figure covers the frequency range $0 < \nu < 250\ cm^{-1}$. The upper plot is for the dispiration near the end of the C-21 chain, and the lower plot is for the same defect, but located near the middle of the C-21 chain. These plots show the existence of a group of normal modes in the frequency range below 110 cm^{-1} which is attributed to the lowest longitudinal frequency of the defect. This group which is indicated by the shaded part of *Figure 12*, is seen to occupy the same frequency range for both positions of the defect in the stem. On the other hand, intensities at frequencies above 110 cm^{-1} tend to strongly depend on the defect location in the stem. If we sum the intensities in *Figure 12* in the entire frequency range shown therein, the resulting sum is almost equal to the intensity of the LAM-1 frequency of the zigzag C-21. This constancy of the sum of intensities agrees well with the experimental finding of Snyder and Scherer[17].

Can the predicted Raman bands, at frequencies around the lowest longitudinal frequency of the defect, be observed in the experimental spectra? Perhaps. *Figure 13* shows the low frequency portion of the Raman spectrum of crystalline polyethylene. The data in this Figure are taken from ref. 8. One notices that, near a band at 108 cm^{-1}, which is attributed to the rotational lattice vibrations of the chain about its axis, there is an intense irregular background. This background might be attributed to the presence of defects, which provide a way of coupling the light waves and lattice vibrations that is not possible in a perfect crystal. The data in *Figure 12* and the supporting normal mode calculations lead to the following conclusions. In oligomers, there are two kinds of contributions to the Raman intensities; those which depend on the defect position in the chain and those which are independent of it. The independent ones, which originate in the defect and the carbon atoms nearby, occupy the frequency range 110 to 85 cm^{-1}. In short chains, on which our calculations are based, the modes with Raman intensities which are dependent on the defect position are in the frequency range above the range associated with the lowest longitudinal frequency of the defects. In long chains, these position-dependent Raman intensities will be at lower frequencies. Normal coordinate analysis provides the following argument in support of this conclusion. Longitudinal waves of the vibrating zigzag segments which are coupled to a defect and which contribute to the calculated high Raman intensities are associated with displacements which form a monotonic

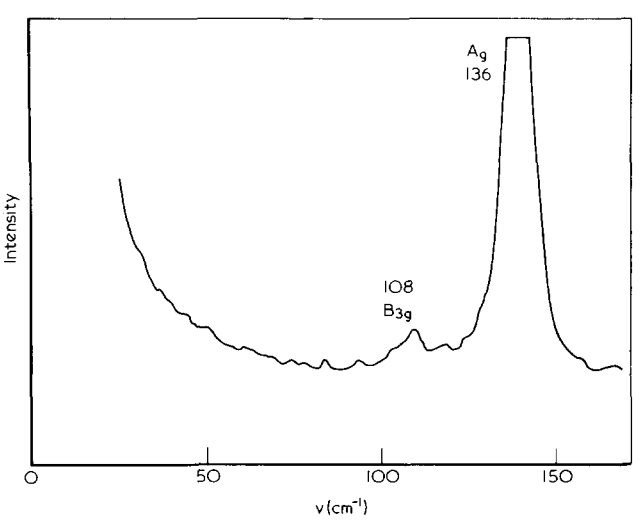

Figure 13 Low frequency Raman spectrum of polyethylene. Data taken from ref. 8

function of the atomic position along the chain axis. These longitudinal waves start at one of the two chain ends and terminate at the defect. The frequency of these longitudinal modes is near the frequency for LAM-1 of the zigzag oligomer having the same length as the length of the longitudinally vibrating zigzag segment in the coupled system. When the defect is near one end of the oligomer, the longitudinally vibrating segment is longer and the associated Raman intensity will be at lower frequency, than is the case for the defect occupying the middle part of the chain. *Figure 12* illustrates this fact. The Raman intensity at $\nu = 175\ cm^{-1}$, lower plot, and the Raman intensity at $\nu = 220\ cm^{-1}$, upper plot, are associated with longitudinally vibrating zigzag segments.

The classification of the low-frequency Raman intensities presented above holds also for long chains. However, since the Raman intensities are inversely proportional to the index of LAM, the intensities which depend on the defect position, that is, which originate from the longitudinally vibrating zigzag segments, will tend to be grouped near the LAM-1 frequency of the zigzag chain with the same number of C atoms.

Currently, calculations are being performed on infra-red intensities of polyethylene. The purpose of these calculations is to determine whether there is evidence for defect related infra-red activity, in particular at low frequency range investigated in this work.

CONCLUSIONS

Defects have a lowest longitudinal frequency that is associated with the motions of the atoms within the defect parallel to the stem axis. Defect vibrations couple to lattice vibrations. Attaching stems to a defect significantly lowers the frequency of a bare defect. This frequency lowering is attributed to the mass perturbation effects of the coupled stems.

The lowest longitudinal frequency of a defect imbedded in a crystal can, in a long stem, find many modes of the zigzag segment which vibrate with nearby frequencies. The lowest longitudinal frequencies of dispirations, disclinations and dislocations in a single stem lay in the range $85\ cm^{-1}$–$105\ cm^{-1}$. This is a consequence of the similarity in lengths, masses and effective moduli for these defects.

The normal coordinate analysis described in this paper leads to the suggestion that defects provide coupling between light waves and the lattice modes that affect the Raman spectra, but would not be seen in the absence of the defects.

The principal effect of the defects on the Raman spectra is in the vicinity of $100\ cm^{-1}$, probably as an increase in the baseline or as the presence of wide and weak bands.

ACKNOWLEDGEMENTS

The authors wish to thank their colleagues, Dr B. Fanconi and Dr R. Rubin, for helpful discussions on various aspects of the work. Special appreciation is extended to Dr E. Bromberg of the Applied Mathematics Division, NBS, for his help in providing for the graphical presentation of the displacement amplitudes.

REFERENCES

1 Reneker, D. H. and Mazur, J. *Polymer* 1983, **24**, 1387
2 Reneker, D. H. and Fanconi, B. *J. Appl. Phys.* 1975, **46**, 4144
3 Koenig, J. L. and Tabb, D. L. *J. Macromol. Sci. Phys. Edn.* 1974, **9**, 141
4 Snyder, R. G., Scherer, J. R., Reneker, D. H. and Colson, J. R. *Polymer* 1982, **23**, 1286
5 McCullough, R. L., Eisenstein, A. J. and Weikert, D. F. *J. Polym. Sci. Phys. Edn.* 1977, **15**, 1837
6 Barnes, J. and Fanconi, B. *J. Phys. Chem. Ref. Data* 1978, **7**, 1309
7 Kitagawa, T. and Miyazawa, T. in 'Advances in Polymer Science', Springer-Verlag, Berlin–New York, 1972, Vol. 9, pp. 335–414
8 Harley, R. T., Hayes, W. and Twisleton, J. F. *J. Phys. Solid State Phys.* 1973, **6**, 167
9 Reneker, D. H., Fanconi, B. M. and Mazur, J. *J. Appl. Phys.* 1977, **48**, 4032
10 Fanconi, B. M. and Crissman, J. *J. Polym. Sci. Polym. Lett. Edn.* 1975, **13**, 421
11 Hsu, S. L. and Krimm, S. *J. Appl. Phys.* 1977, **48**, 4013
12 Ullersma, P. and Tjon, J. A. *Physica* 1974, **71**, 294
13 Strobl, G. R. *J. Polym. Sci. Polym. Phys. Edn.* 1983, **21**, 1357
14 Takeuchi, H., Shimanouchi, T., Tasumi, M., Vergoten, G. and Fleury, G. *Chem. Phys. Lett.* 1974, **28**, 449
15 Mazur, J. and Fanconi, B. *J. Chem. Phys.* 1979, **71**, 5069
16 Bright-Wilson, E., Decius, J. C. and Cross, P. C. in 'Molecular Vibrations', McGraw-Hill, New York, NY (1955)
17 Snyder, R. G. and Scherer, J. R. *J. Polym. Sci. Polym. Phys. Edn.* 1980, **18**, 428